Theoretical analysis of a dynamic thermoconvective pattern in a circular container

P. C. Dauby*
Université de Liège, Institut de Physique B5, B-4000 Liège 1, Belgium

P. Colinet†
Microgravity Research Center (MRC), Université Libre de Bruxelles, CP 165/62, avenue F. D. Roosevelt, 50, 1050 Bruxelles, Belgium

D. Johnson
Department of Chemical Engineering, The University of Alabama, A 134 Bevill Building, Box 870203, Tuscaloosa, Alabama 35487-0203
(Received 13 September 1999)

The gravity- and surface-tension-driven thermoconvective instability of a fluid layer contained in a no-slip circular container of aspect ratio 2.5 is investigated. Linear and nonlinear analyses are developed. From amplitude equations the bifurcation diagram of the system is deduced, and the different stable convective patterns are studied. In particular, it is shown that a stable heteroclinic cycle due to a 1-2 spatial resonance is predicted. This cycle is also shown to be in agreement with recent experimental observations of a dynamic mode switching.

PACS number(s): 47.20.−k, 05.45.−a, 44.25.+f, 47.27.Te

I. INTRODUCTION

Pattern formation is an important subject of fluid mechanics. In particular, Rayleigh-Bénard-Marangoni thermoconvective instabilities have interested many researchers for about a century. Interesting reviews and bibliography on this problem can be found, for instance, in the book by Koschmieder [1] or in Ref. [2].

When a horizontal liquid layer is heated from below, it is well known that convection sets in provided the temperature difference between the bottom and top of the system is larger than some critical value. In horizontally infinite layers the instability is most often stationary [3], and a steady regular structure of hexagonal, square, or roll-like convective cells is observed above the threshold [4–6]. However, when the liquid layer is confined in small containers with vertical sidewalls, fascinating nonsteady behaviors have also been discovered in experiments quite recently. In Ref. [7], Ondarçuhu *et al.* report observations of three kinds of oscillating patterns in a square container with aspect ratio (width over heigth) 4.6. These dynamic behaviors are related by the authors to the presence of a Takens-Bogdanov bifurcation in the system.

More recently, in a circular container with aspect ratio (radius over height) equal to 2.5, a dynamic mode switching between two two-cell patterns related by a $\pi/2$ rotation about the vertical symmetry axis of the system was observed [8]. In this experiment, the fluid was lying below an air layer so that both the gravity and the surface-tension variations with temperature were active in the instability mechanism (''Rayleigh-Bénard-Marangoni instability'').

In the present paper, we propose a theoretical analysis of this mode switching. More precisely, we show that the dynamics of the system can be described by amplitude equations forming a low-dimensional system of ordinary differential equations whose bifurcations give rise to the same dynamic behavior as that seen in experiments [8].

Thermoconvective instabilities in confined domains have already been studied theoretically by several authors. The different works can be classified into two broad categories, depending on the type of boundary conditions used for the velocity along the sidewalls. In Refs. [9–12], the sidewalls of the containers are assumed to be ''slippery,'' or, more precisely, ''vorticity free,'' while more realistic no-slip walls were considered, for instance, in Refs. [13–17] (see also the references from these papers). The model of slippery walls is quite convenient since it enables a complete separation of the vertical and horizontal space coordinates in the equations. In a very interesting paper [12], Echebarría, Krmpotić, and Pérez-García described dynamic solutions in such containers. Their analysis showed the possibility of nonstationary behaviors (rotating waves, modulated rotating waves or heteroclinic orbit) resulting from a 1-2 spatial resonance of two different modes of convection. The purpose of the present work is to extend their approach to realistic no-slip sidewalls, and to compare the theoretical predictions with experiments.

II. BASIC EQUATIONS

The basic equations of the problem in the frame of the Boussinesq approximation are well known. Considering the perturbations with respect to a conductive state, these equations read

$$\nabla \cdot \mathbf{u} = 0, \tag{1}$$

$$\mathrm{Pr}^{-1}[\partial_t \mathbf{u} + \mathbf{u} \cdot \nabla \mathbf{u}] = -\nabla p + \triangle \mathbf{u} + \mathrm{Ra}\, T \mathbf{e_z}, \tag{2}$$

$$\partial_t T + \mathbf{u} \cdot \nabla T - w = \triangle T. \tag{3}$$

*Electronic address: PC.Dauby@ulg.ac.be
†Also at Instituto Pluridisciplinar, Universitad Complutense de Madrid, Paseo Juan XXIII 1, 28040 Madrid, Spain.

We have chosen a vertical z axis in the direction opposite to gravity. The equations are written in a nondimensional form with distances scaled by d, the thickness of the liquid layer. The time scale is given by d^2/κ, with κ the heat diffusivity of the liquid. The temperature scale is chosen as βd, with β the vertical temperature gradient within the liquid layer in a purely conductive state, and the velocity is scaled by κ/d. Symbols $\mathbf{u}=(u,v,w)$, p, and T represent the nondimensional velocity, pressure and temperature perturbed fields. The Rayleigh and Prandtl numbers Ra and Pr are defined as

$$\mathrm{Ra}=\frac{g\alpha\beta d^4}{\nu\kappa}, \tag{4}$$

$$\mathrm{Pr}=\frac{\nu}{\kappa}, \tag{5}$$

where ν and α are the liquid kinematic viscosity and coefficient of thermal expansion.

The boundary conditions at the bottom of the box ($z=0$) express that the wall is rigid and perfectly heat conducting. The upper free surface ($z=1$) is assumed to remain undeformed, while the surface tension is supposed to be a linear function of temperature. The heat transfer is modeled using a Biot condition. The mathematical expressions for these conditions are

$$\mathbf{u}=T=0 \quad \text{at } z=0, \tag{6}$$

$$w=\frac{\partial T}{\partial z}+\mathrm{Bi}\,T=0 \quad \text{at } z=1, \tag{7}$$

$$\frac{\partial u}{\partial z}+\mathrm{Ma}\frac{\partial T}{\partial r}=\frac{\partial v}{\partial z}+\mathrm{Ma}\,r^{-1}\frac{\partial T}{\partial \phi}=0 \quad \text{at } z=1, \tag{8}$$

where r and ϕ are the horizontal polar coordinates. The Marangoni number Ma, given by

$$\mathrm{Ma}=\frac{\gamma\beta d^2}{\rho\nu\kappa}, \tag{9}$$

is expressed in terms of γ, the sign-changed derivative of surface tension with respect to temperature, and the fluid mass density ρ.

The lateral sidewalls are rigid and insulating so that one has

$$\mathbf{u}=\frac{\partial T}{\partial r}=0 \quad \text{at } r=a, \tag{10}$$

where a is the aspect ratio of the container.

III. LINEAR STABILITY ANALYSIS

A general linear stability analysis for this problem was carried out in Ref. [17]. Only the results needed later are given in Fig. 1, where the critical nondimensional temperature difference λ_c, defined as

$$\lambda_c=\frac{\mathrm{Ra}_c}{669}+\frac{\mathrm{Ma}_c}{79.6}, \tag{11}$$

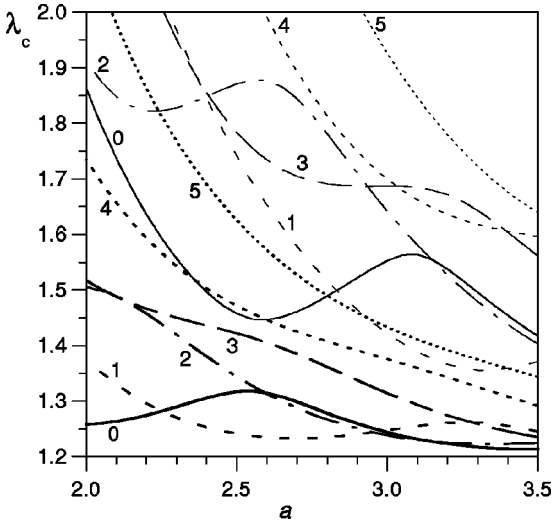

FIG. 1. Critical nondimensional temperature difference vs aspect ratio. The first and second eigenvalues are represented as thick and thin lines. The value of the azimuthal wave number m is indicated on each curve.

is plotted as a function of the aspect ratio a, for a in the neighborhood of 2.5 (Ra_c and Ma_c are the critical Rayleigh and Marangoni numbers). In the calculations leading to these curves, as well as in the other results presented in this paper, the thickness of the liquid layer is 5 mm (a is varied by changing the radius of the container). The viscosity of the fluid is 1 S (10^{-4} m^2 s^{-1}), and the Prandtl number is equal to 1000. The air layer above the liquid has a depth equal to half of the depth of the liquid layer, so that the air layer can be considered as purely conductive [3,18,19]. An equivalent Biot number can then be defined by using Eq. (4.1) in Ref. [16]. With conductivities for the air and for the liquid being 0.026 and 0.16 W m^{-1} K^{-1}, respectively, this Biot number is equal to 0.43. The negative of the derivative of surface tension with respect to temperature is equal to 5×10^{-5} N m^{-1} K^{-1}, and the density of the liquid is 968 kg m^{-3}. The coefficient of thermal expansion is fixed to 9.6×10^{-4} K^{-1}. The above values for the different quantities are chosen in order to correspond to the experiments reported in Ref. [8], except that the thickness of the air layer is smaller in order to ensure that the upper gas remains mechanically passive [3].

The different curves in Fig. 1 correspond to different values of the azimuthal wave number m. For each m, thick and thin lines are used to represent the threshold of the first and second eigenmodes, respectively. In the neighborhood of $a=2.5$, the convective threshold is characterized by an $m=1$ pattern. For $a=2.5$, λ_c is equal to 1.24, while the critical Rayleigh and Marangoni numbers are given by 292 and 64.1, respectively. A codimension-two point appears at $a=2.961$. For this aspect ratio, the $m=1$ and 2 critical curves intersect, and the two modes are simultaneously unstable. Note that the $m=0$ mode becomes unstable quite close to the instability threshold of the $m=1$ and 2 patterns. It is important to mention that these results are quite different from those obtained under the assumption of slippery lateral walls (see, for instance, Fig. 1 in Ref. [12]). In particular, the $m=0$ curve for slippery walls is quite far from the intersection of the other

two modes. Moreover, the aspect ratio giving rise to the codimension-two point is much smaller ($a \approx 1.15$) than ours.

IV. NONLINEAR THERMOCONVECTION FOR $a=2.5$

The second step of our analysis is devoted to a description of the system above the convective threshold, i.e., in the nonlinear regime. The method consists in reducing the dynamics of the system to the dynamics of the most unstable modes. The procedure is completely similar to that presented in Ref. [16] for the study of rectangular no-slip containers and will be summarized only very shortly. The solution of the nonlinear partial differential equations system is first expanded in a series of the eigenmodes of the linear problem. These eigenmodes are numerically obtained by fixing the temperature difference across the liquid to its critical value and by considering the linear growth rate as the eigenvalue. In the weakly nonlinear regime, the dynamics of the system is dominated by the dynamics of the most unstable modes of convection with the largest growth rates. A careful examination of the numerical data corresponding to Fig. 1 shows that for $a=2.5$, the first $m=0$, 2, and 3 modes (thick lines) become successively linearly unstable for relative distances to the threshold [$\epsilon=(\lambda-\lambda_c)/\lambda_c$)] equal to 6.37×10^{-2}, 8.53×10^{-2}, and 15.47×10^{-2}. All the other modes become unstable for still larger values of ϵ. Therefore we choose the $m=0$, 1, and 2 modes as the most unstable convective patterns, or ''active'' modes, whose interactions determine the weakly nonlinear behavior of the fluid layer. The so-called amplitude equations are then obtained by a standard slaving principle (see, for instance, Ref. [16]), for which the slaved modes are all the (nonactive) eigenmodes with a linear growth rate larger than -50 and with an azimuthal wave number m between 0 and 4; all the other modes are simply disregarded. The validity and convergence of this procedure will be discussed briefly later on. The obtained system of equations for the complex amplitudes A_0, A_1, and A_2 of the $m=0$, 1, and 2, modes is the following:

$$\dot{A}_0=(l_0\epsilon+\sigma_0)A_0+q_{000}A_0^2+q_{011}|A_1|^2+q_{022}|A_2|^2+c_{0000}A_0^3+c_{0011}A_0|A_1|^2+c_{0022}A_0|A_2|^2+c_{0112}(A_1^2A_2^\star+A_2A_1^{\star 2}), \tag{12}$$

$$\dot{A}_1=(l_1\epsilon+\sigma_1)A_1+q_{101}A_0A_1+q_{112}A_1^\star A_2+c_{1001}A_0^2A_1+c_{1012}A_0A_1^\star A_2+c_{1111}|A_1|^2A_1+c_{1221}|A_2|^2A_1, \tag{13}$$

$$\dot{A}_2=(l_2\epsilon+\sigma_2)A_2+q_{202}A_0A_2+q_{211}A_1^2+c_{2002}A_0^2A_2+c_{2011}A_0A_1^2+c_{2112}|A_1|^2A_2+c_{2222}|A_2|^2A_2. \tag{14}$$

The values of the different coefficients in these equations are given in Table I (the normalization condition used for the eigenmodes was given in Ref. [17]). Equations (12)–(14) describe the interactions of the three modes $m=0$, 1, and 2 in the neighborhood of the threshold. When polar coordinates are used for the complex amplitudes, the rotational invariance of the physical system allows the removal of one of the two phase variables. The equilibrium solutions of this reduced system correspond for the real physical system either to stationary solutions or to traveling (rotating) waves [12]. A standard bifurcation analysis using AUTO97 software was carried out on this system. The bifurcation diagram is given in Fig. 2, where the full and dashed lines represent the stable and unstable solutions, respectively. At $\epsilon=0$ (point B_1), the $m=1$ mode bifurcates supercritically. Its nonlinear autointeraction generates the $m=0$ and 2 modes, so that the complete pattern is a superposition of the three modes. The convective pattern of this mixed mode solution M_1 is depicted in Fig. 3, where the vertical velocity at middepth of the container is plotted. The primary bifurcations of the $m=0$ and 2 modes at $\epsilon=6.37\times10^{-2}$ (point B_0) and 8.53×10^{-2} (point B_2) do not give rise to stable solutions. On the M_1 branch, thanks to a secondary bifurcation, another stable solution which corresponds to a rotating wave (RW) pattern appears. This RW pattern exists only for a small range of ϵ, between 31.7×10^{-2} and 33.0×10^{-2}. The rotating pattern is also a superposition of the three elementary modes and is represented in Fig. 4. The period of rotation is 126 (nondimensional time) for $\epsilon=32.8\times10^{-2}$. For the silicon oil used in the experiments [8], the dimensional period is then around 10 h, so that the rotation is quite slow. The RW branch loses stability at $\epsilon=33.0\times10^{-2}$ due to a Hopf bifurcation. This bifurcation is subcritical and no stable modulated wave

TABLE I. Values of the coefficients of the amplitude equations.

A_0		A_1		A_2	
l_0	5.83	l_1	7.63	l_2	8.32
σ_0	−0.372	σ_1	0.00	σ_2	−0.710
q_{000}	1.89	q_{101}	0.742	q_{202}	−1.64
q_{011}	17.1	q_{112}	9.89	q_{211}	1.02
q_{022}	17.0				
c_{0000}	−26.4	c_{1001}	−24.5	c_{2002}	−9.99
c_{0011}	−137.	c_{1012}	−33.1	c_{2011}	−27.0
c_{0022}	−180.	c_{1111}	−106.	c_{2112}	−164.
c_{0112}	8.95	c_{1221}	−106.	c_{2222}	−71.8

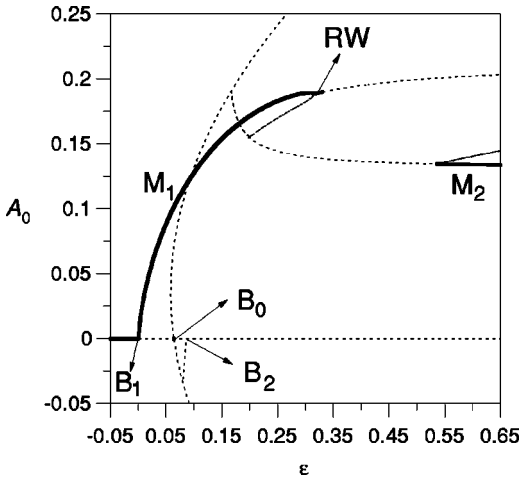

FIG. 2. Bifurcation diagram for $a=2.5$. The amplitude A_0 of the $m=0$ mode is represented as a function of the relative distance to the threshold ϵ. Stable and unstable branches are represented by full and dashed lines. B_1, B_0, and B_2 indicate the primary bifurcation points for the $m=1$, $m=0$, and $m=2$ modes.

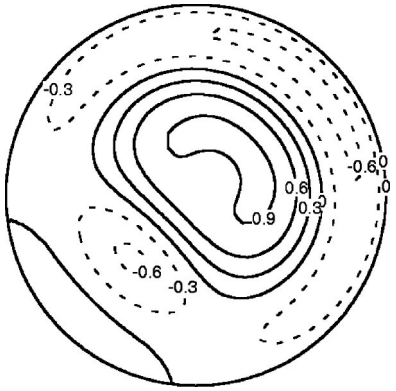

FIG. 3. Vertical velocity at middepth for the M_1 solution ($\epsilon = 15\times10^{-2}$).

(MW) can be observed. From this bifurcation point until $\epsilon = 53.5\times10^{-2}$, no stationary solution exists for the reduced system. Numerical integrations have shown that in this ϵ range, a stable heteroclinic orbit exists. This heteroclinic orbit is due to the spatial nonlinear resonance of the $m=1$ and 2 modes, as already discussed by several authors [12,20–22]. For this solution, the role of imperfections in the system is known to make the heteroclinic orbit periodic, with a period which decreases when imperfections are becoming more important. In experiments, a possible imperfection originates from the fact that the container is never perfectly horizontal. For this reason, the $m=1$ convective mode always has a small, but nonvanishing, amplitude. In the numerical calculations, these imperfections can easily be introduced by artificially adding a small constant term to the right-hand side of Eq. (13). Note, however, that this term must not necessarily be introduced into the description, since the numerical noise, which prevents the right-hand side from becoming exactly zero, is in fact sufficient for giving the heteroclinic orbit a finite period.

The periodic solution for the imperfect system is characterized by the alternation of two quasistationary patterns which are rotated by $\pi/2$ with respect to each other. For each of these patterns, two convective cells are observed during very long time intervals. These cells result from a superposition of the $m=2$ and 0 modes, while A_1 remains very small. The transition from one pattern to the other is induced by a sudden increase of A_1, which gives rise to a corresponding increase in size of one of the two cells. Then for a short time, the pattern consists of a unique cell that finally splits into the two cells of the rotated pattern. In Fig. 5, the time evolution of the amplitudes is shown (recall that the precise value of the period depends on the imperfections or on the precision of the calculations). Figure 6 presents the time evolution of the convective pattern during one period. Finally, let us recall that if no constant term is added to Eq. (13) for the numerical calculations, the machine epsilon plays the role of the imperfection but its sign is undetermined. As a consequence, the transition between the two two-cell patterns has no fixed direction since any of the two cells can grow before splitting. This numerical solution with no explicit imperfection is thus not, strictly speaking, periodic (noise-induced chaos).

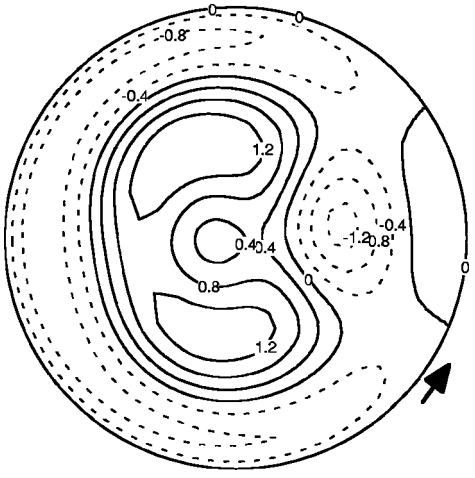

FIG. 4. Vertical velocity at middepth for the rotating wave ($\epsilon = 32.8\times10^{-2}$).

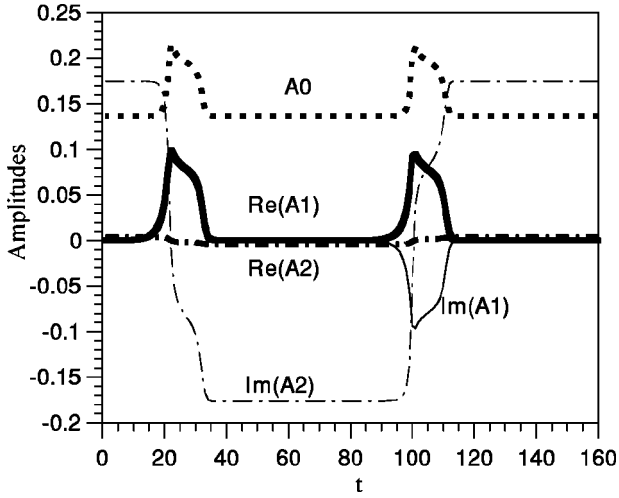

FIG. 5. Time evolution of the amplitudes for the heteroclinic orbit ($\epsilon = 40\times10^{-2}$).

The last stable solution of Eqs. (12)–(14) appears in the bifurcation diagram at $\epsilon = 53.5\times10^{-2}$. At this point, the quasistationary part of the heteroclinic orbit (the two-cell structure) becomes stable, with a zero value for A_1. This solution is a superposition of the $m=2$ and 0 modes (mixed modes M_2) and is represented in Fig. 7.

To end this section, we discuss briefly the convergence of the bifurcation diagram when the number of modes taken into account in the description is increased. First we have checked that when the number of slaved modes is increased by decreasing the minimum linear growth rate below -50, the values of the coefficients given in Table I actually converge. The second important verification is carried out by writing amplitude equations not only for the most unstable three modes as in Eqs. (12)–(14), but also for modes with higher azimuthal wave numbers or for modes corresponding to the second or the third eigenvalue for a given m. In all cases, we have observed that the bifurcation diagrams for the more complex system give rise to the same transitions with the same stable convective patterns.

V. DISCUSSION AND CONCLUSION

In this work we have studied the nonlinear Rayleigh-Bénard-Marangoni thermoconvection within a circular con-

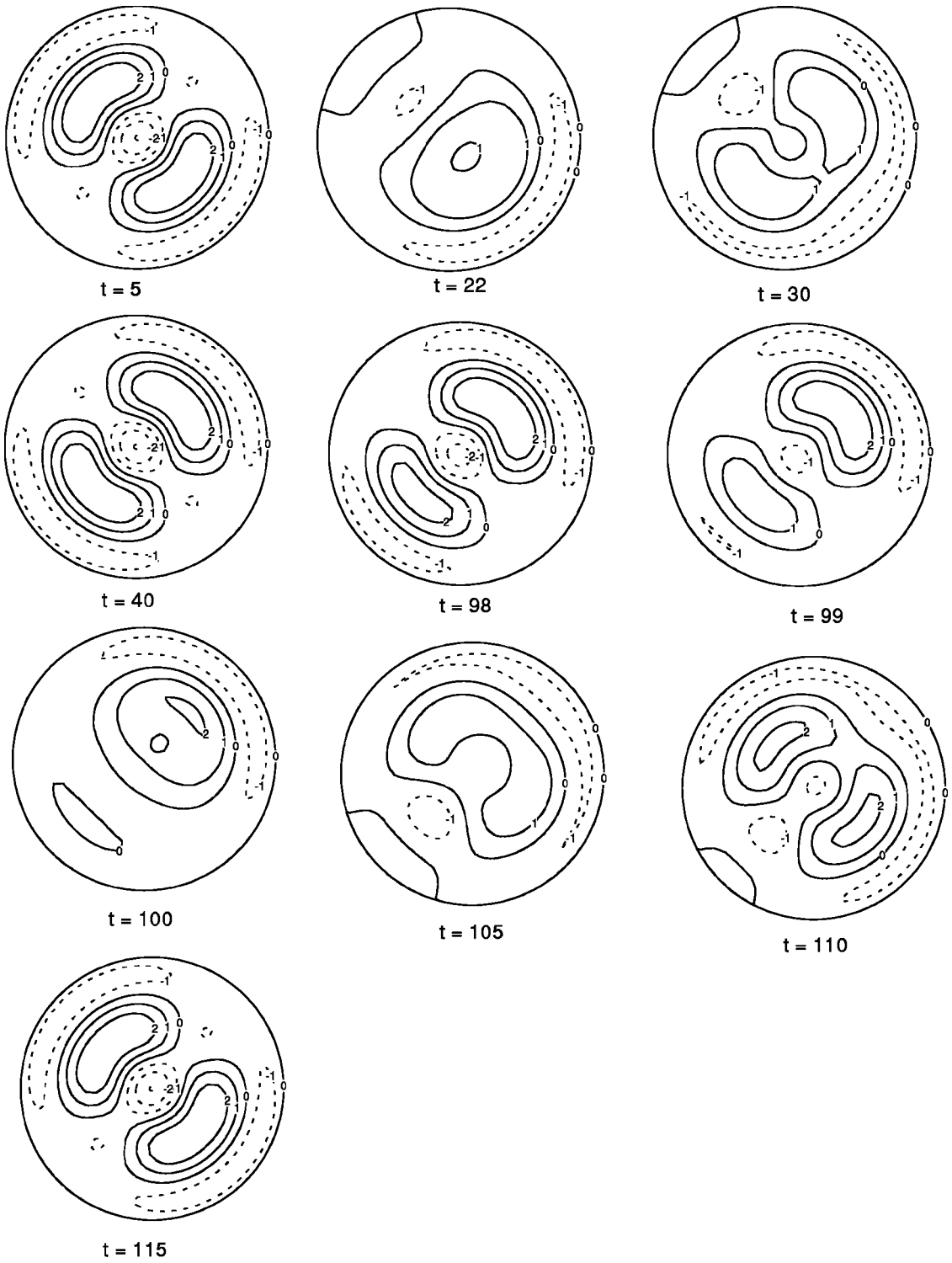

FIG. 6. Vertical velocity at middepth for the heteroclinic orbit ($\epsilon = 40 \times 10^{-2}$). The time t corresponds to the abscissa in Fig. 5.

tainer of aspect ratio 2.5. We have shown that different convective patterns can appear in the heated fluid, depending on the distance to the threshold. Just above the linear stability threshold, a one-cell solution is displayed (mixed mode M_1, Fig. 3). For larger values of the distance to the threshold, a rotating one-cell solution is stable (rotating wave RW, Fig. 4). Note, however, that the stability range on the ϵ axis for this rotating pattern is very small. For this reason, this convective structure should be quite delicate to observe in experiments (and is indeed not mentioned in [8]). For the highest values of ϵ investigated here, a stable steady pattern can be observed which is made up by two symmetric convective cells (mixed modes M_2, Fig. 7). For distances to the threshold larger than the upper limit for the rotating wave and smaller than the lower limit for the M_2 solution, no stationary solution exists. The behavior of the fluid becomes dynamic and takes the form of a stable heteroclinic orbit (Fig. 6). This solution is characterized by a switching between two two-cell patterns rotated by $\pi/2$ with respect to each other. It is important to note that this mode switching is completely

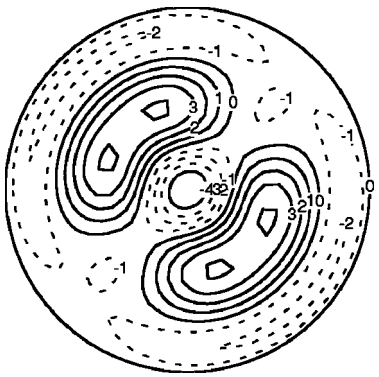

FIG. 7. Vertical velocity at middepth for the M_2 solution ($\epsilon = 55\times 10^{-2}$).

similar to the experimental observations of Johnson and Narayanan (see Fig. 2 in Ref. [8]). In their work, these authors sensed that this dynamic behavior of the fluid had to be attributed to the presence of a codimension-2 point, for which the $m=2$ and 0 modes are simultaneously unstable. The present analysis definitely shows that the codimension-2 point is actually present in the system, but the $m=1$ and 2 modes collaborate to generate the spatial resonance and the heteroclinic orbit. This kind of heteroclinic behavior is of course important in the context of the study of the transitions to complex behaviors in dynamical systems, and has already been considered by several authors in the past (see, for instance Refs. [12,20–23], and references therein). In particular, we have already mentioned that Echebarría, Krmpotić, and Pérez-García already described the possibility of such heteroclinic cycles in the case of slippery containers [12]. However, the aspect ratio they predicted for this behavior is not the same as in experiments, and the corresponding convective patterns are also different from the experimental structures, especially along the vertical walls. Note also that the MW which can be stable in slippery containers is unstable in our analysis. In the present work, more realistic no-slip lateral walls are taken into account and it is shown that the heteroclinic orbit is still present. To our knowledge, this analysis provides the first example of a real and nonacademic physical system for which both experiments and a rigorous theoretical analysis show the presence of a heteroclinic connection.

ACKNOWLEDGMENTS

We are pleased to thank Professor R. Narayanan (University of Florida), Professor G. Lebon (Liège University), Professor C. Pérez-García (Universitad de Navarra), and Dr. B. Echebarría (Northwestern University) for interesting comments and suggestions. P.C.D. is pleased to acknowledge NATO for financial support, and Professor R. Narayanan for his kind hospitality at the University of Florida in Gainesville. During part of this work, P.C. benefited from the support of the EC through Marie Curie Research Grant No. ERBFMBICT972099. This text presents results of the Belgian Program InterUniversity Pole of Attraction (IUPA 4-06) initiated by the Belgian State, Prime Minister's Office, Federal Office for Scientific, Technical and Cultural Affairs.

[1] E. L. Koschmieder, *Bénard Cells and Taylor Vortices* (Cambridge University Press, Cambridge, 1993).
[2] P. Colinet, Ph. D. thesis, ULB, Belgium, 1997.
[3] V. Regnier, P. C. Dauby, and G. Lebon (unpublished).
[4] P. Parmentier, V. C. Regnier, G. Lebon, and J. C. Legros, Phys. Rev. E **54**, 411 (1996).
[5] V. Regnier, P. C. Dauby, P. Parmentier, and G. Lebon, Phys. Rev. E **55**, 6860 (1997).
[6] K. Eckert, M. Bestehorn, and A. Thess, J. Fluid Mech. **356**, 155 (1998).
[7] T. Ondarçuhu, G. B. Mindlin, H. L. Mancini, and C. Pérez-García, Phys. Rev. Lett. **70**, 3892 (1993).
[8] D. Johnson and R. Narayanan, Phys. Rev. E **54**, R3102 (1996).
[9] S. Rosenblat, S. H. Davis, and G. M. Homsy, J. Fluid Mech. **120**, 91 (1982).
[10] S. Rosenblat, G. M. Homsy, and S. H. Davis, J. Fluid Mech. **120**, 120 (1982).
[11] P. C. Dauby, G. Lebon, P. Colinet and J. C. Legros, Q. J. Mech. Appl. Math. **46**, 683 (1993).
[12] B. Echebarría, D. Krmpotić, and C. Pérez-García, Physica D **99**, 487 (1997).
[13] G. R. Hardin, R. L. Sani, D. Henry, and B. Roux, Int. J. Numer. Methods Fluids **10**, 79 (1990).
[14] J. -C. Chen, J. -Y. Chen, and Z. -C. Hong (unpublished).
[15] H. A. Dijkstra, Microgravity Sci. Technol. **VII**, 307 (1995); **VIII**, 70 (1995); **VIII**, 155 (1995).
[16] P. C. Dauby and G. Lebon, J. Fluid Mech. **329**, 25 (1996).
[17] P. C. Dauby, G. Lebon, and E. Bouhy, Phys. Rev. E **56**, 520 (1997).
[18] D. Johnson, R. Narayanan, and P. C. Dauby, in *Fluid Dynamics at Interfaces*, edited by W. Shy and R. Narayanan (Cambridge University Press, Cambridge, 1999).
[19] C. Pérez-García, B. Echebarría, and M. Bestehorn, Phys. Rev. E **57**, 475 (1998).
[20] M. R. E. Proctor and C. A. Jones, J. Fluid Mech. **188**, 301 (1988).
[21] D. Armbruster, J. Guckenheimer, and P. Holmes, Physica D **29**, 257 (1988).
[22] P. Holmes, J. L. Lumley, and G. Berkooz, *Turbulence, Coherent Structures, Dynamical Systems and Symmetry* (Cambridge University Press, Cambridge, 1996).
[23] M. Krupa, J. Nonlinear Sci. **7**, 129 (1997).